AN ACCURATE TEMPERATURE REGULATING SCHEME BASED ON A RESISTOR WITH TAILORED NONLINEARITY FOR EVAPORATIVE DRUG DELIVERY

Frank Goldschmidtboeing[1], Mohammadreza Saberi[1], Timo Gerach[1], Luca Conrad[1], Eiko Hager[1], Uttunga Shinde[1], Muhannad Ghanam[1], Uwe Pelz[1], Niklas Romming[2], Lasse Cornils[2], Jan Jaklin[2], Marc Kessler[2] and Peter Woias[1]*

[1]University of Freiburg, Freiburg, Germany

[2]Hauni Maschinenbau GmbH, Hamburg, Germany

ABSTRACT

We present the temperature regulation scheme of a resistive silicon heater for evaporative drug delivery to the lungs. The nonlinear specific resistance to temperature behavior of boron doped silicon is used to enable an absolute temperature measurement of the heater without the need of a calibration procedure. Experiments demonstrate that the evaporated mass can be controlled by the heater temperature. The evaporated mass versus heater temperature is linear in the region of useful heater temperatures.

KEYWORDS

evaporative drug delivery to the lungs, silicon resistive heater, nonlinear specific resistance to temperature curve

INTRODUCTION

Evaporation of medical substances has been identified as a promising route for future drug delivery to the lungs [1,2,3,4]. This application demands a reliable temperature control to avoid overheating and thereby destroying the medical substance. A high dosing accuracy is needed to guarantee proper dosing of the drug. A MEMS-based silicon device to fulfill these requirements has been demonstrated in [5], where the basic function of our device was shown. Here, we show a temperature regulations scheme, that guarantees an accurate temperature control of the silicon heating component even with varying initial resistance of the heating element and simultaneously varying ambient temperature.

SYSTEM DESIGN AND FABRICATION

A schematic of the evaporation device is shown in Fig. 1. It consists of an electronic steering device, that powers the heater and regulates its temperature and the disposable drug reservoir with the resistive heater and mouth piece as a vapor outlet.

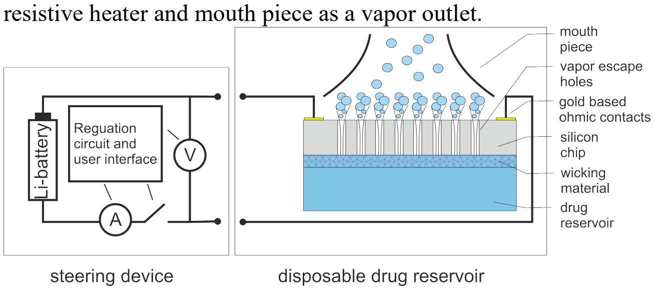

Figure 1: Schematic of the evaporation device

The resistor is directly driven by a rechargeable lithium ion battery with a nominal voltage of 3.7 V. A low resistance MOSFET is used to switch the power delivered to the heater on and off according to the measured resistance of the heater. The resistance of the heater is about 1.2 Ω when heated to the evaporation temperature, therefore, with a nominal voltage of 3.7V a maximum instantaneous power of 11.4 W can be delivered to the heater.

The heater current and voltage are measured every 2 ms allowing to determine the instantaneous power and the actual resistance of the heater. Two regulation algorithms can be chosen. The first algorithm regulates the temperature to a pre-set value by a two-point regulation scheme. The heater is switched off, as soon as the resistance (temperature) reaches a threshold and switches on again if it falls below a second, slightly smaller threshold..In this case the average input power can be evaluated as parameter describing the status of the heating device. In the following this algorithm will be called temperature regulation algorithm.

The second algorithm regulates the input power by determining the average input power of the last few timesteps and by choosing the on or off-state accordingly. Here, the temperature curve can be evaluated as a second parameter describing the evaporation event. This algorithm will be called power regulation in the following.

Both algorithms need a precise temperature measurement by evaluating the instantaneous resistance of the heating element to ensure that no overtemperature on the heater leads to a degradation of the drug or the solvent.

The fabrication of the silicon heater was described in detail in [5]. Fig. 2 shows the silicon heater connected to a flexible PCB by silver sintering. This technology enables stable operation up to temperatures of 300°C.

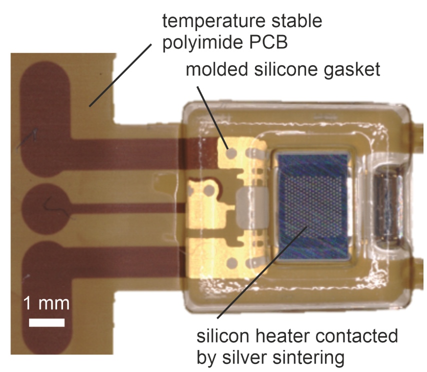

Figure 2: Packaging of the MEMS heater chip

The doping element and level of the MEMS heater were chosen to achieve a total room temperature resistance of 1 Ω with a reasonable aspect ratio of the chip, i.e. a square shaped perforated evaporation area and contacts areas on two sides leading to chip with 3 mm length and 2 mm width. Furthermore, an adapted specific resistance versus temperature curve is required to enable a resistive temperature measurement without prior calibration. The measurement method described in this paper requires a temperature independent resistance at room temperature and a preferably linear temperature dependence in the evaporation range of 200°C to 300°C.

The specific resistance of semiconductors typically decreases with temperature because more carriers are lifted into the conduction band at higher temperatures. A soon as virtually all doping levels are ionized another effect comes into play, further

increase in temperature leads to more carrier scattering and therefore lower carrier mobility, so the resistance increases again. Therefore, a small region of temperature independent resistance, where both effects compete, exists. The above-mentioned criteria are met, if this region can be shifted to room temperature and if a specific resistance value of about 20 mΩcm can be achieved.
We have chosen a boron doping concentration of 4 10^{18} cm^{-3} with a specific resistance obtained from theory [6] shown in Fig. 3.

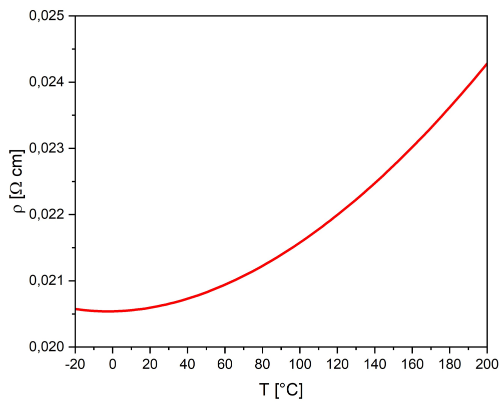

Figure 3: Theoretical specific resistance of boron doped silicon with a concentration of $4 \cdot 10^{18}$ cm^{-3}

MEASUREMENT SETUP

First, measurements were conducted to evaluate the resistance to temperature curve of the fabricated chips. Precise measurements were taken in the temperature range of -20°C to 150°C in a climate chamber with a four-wire measurement setup (Keithley Source Meter 2450). The temperature was raised in steps of 5 K and resistance values were taken after 5 minutes of waiting time to secure thermal equilibration.

Higher temperatures of 160°C to 300°C could only be reached by resistive heating of the chips. For this, the resistance was regulated by the temperature regulation algorithm and the temperature of the chip was measured by the infrared-camera Optris PI 450, Optris GmbH, Berlin Germany. The mean temperature of a center region of the chip was taken as the chip temperature, although the effect of the small holes in the chip might influence its value.

A second set of measurements was done to find the relation of chip temperature, heating power and generated aerosol mass. Fig. 4 shows a schematic of the full measurement set-up while Fig. 5 shows a photograph of the heating device, with the heater cartridge and the filter holder.

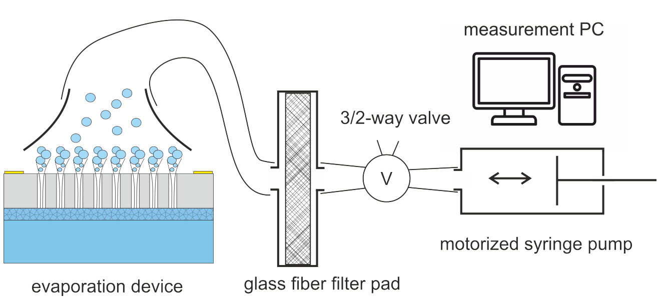

Figure 4: Schematic of the aerosol mass measuring system

In the experiments, the heater is powered for a period of 3s with one of the two regulation algorithms. A drug-free solvent mixture of water, propylene glycol and glycerol is used. The resistance versus time curves for each evaporation event is recorded with a sampling rate of 2 ms. The vapor is generated directly below the heater and escapes through the holes. After that the vapor condenses to an aerosol with a mass median droplet diameter of approximately 1 µm. An air flow of 1.2 l/min is generated by a motor-driven syringe pump and draws the aerosol through a glass fiber filter. A small part of the aerosol droplets hit the tubing and remains there, while the major part condenses inside the filter. The filter is weighted every ten evaporation events to determine the average aerosol mass per event.

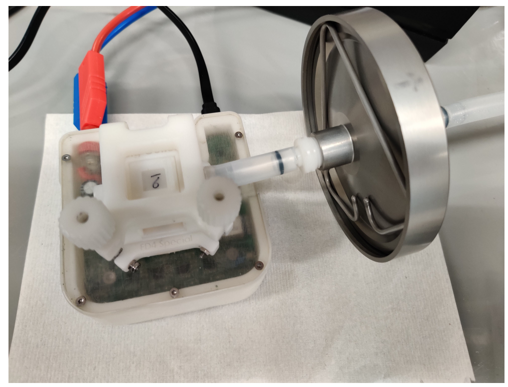

Figure 5: Photograph of the steering electronics (bottom) with a liquid cartridge mounted on top and the filter pad holder connected

RESULTS AND DISCUSSION

The characterization of resistance versus temperature behavior is summarized in Fig. 6. The resistance is scaled by the measured resistance at room temperature and the scaled resistance is denoted by *F*. This scaling compensates for tolerances of the chip dimensions, especially the chip thickness. The measurements in the climate chamber (blue dots and the measurements with the IR-camera align quit well, with a small offset of the IR-camera values to higher temperatures. These IR-camera values also show a higher noise. This noise is due to the different resistance measurement system. The resistance was measured with the miniaturized microcontroller based steering electronics and not with a highly accurate multimeter as in the climate chamber measurements. Also, the temperature measurement is less accurate due to the influence of the tiny holes inside the MEMS heater.

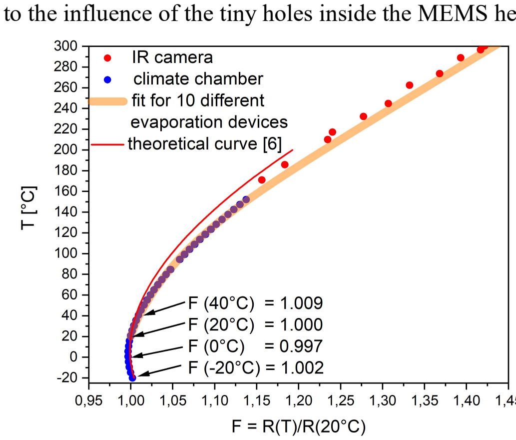

Figure 6: Summary of the measured temperature dependence of the MEMS heaters

The thin red line shows the theoretical specific resistance versus temperature curve from Fig. 3. It fits well to the measured data. The small deviation is probably due to the tolerance of the doping level of the wafers.

The thick orange curve shows a curve fitted to the results of IR-measurements of ten different MEMS heaters and the climate chamber measurement of a single MEMS heater. The IR-measurement points lie all within a margin of ±15 K around this curve, but we assume that the main part of this tolerance is due to the temperature measurement inaccuracy. This orange curve is used for all heaters to determine the heater temperature from the resistance value.

As mentioned above, all measurements are normalized by the room temperature resistance. As this resistance is virtually constant from -20°C to +40°C the exact temperature of this measurement is of no importance. That is why it can be measured at any time by the electronic steering device without any information about the temperature of the liquid cartridge. The different values of F shown in figure 6 demonstrate, that a maximum error of 0.9% occurs at a temperature of 40°C.

The evaporation experiments were conducted with the power regulation algorithm. Fig. 7 shows the aerosol mass versus heating power measured at laboratory temperature of 20°C. Each dot consists of the average data of ten successive evaporation events. An error of ±0.2 mg is assumed for the mass measurement, which is a typical standard deviation when the same MEMS heater is characterized multiple times under the same conditions. The power regulation algorithm regulates the power within a better than 1% accuracy, which makes the error bars smaller than the dots.

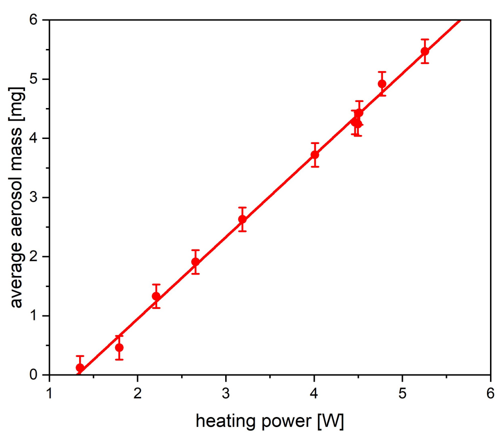

Figure 7: Average aerosol mass versus heating power for ten evaporation events with a duration of 3 s each

The fitted line clearly shows the linear behavior of the aerosol mass versus temperature curve with a small offset. This is to be expected as most of the power is used for heating up the liquid and overcoming the latent heat of evaporation. Nevertheless, there is still an accuracy problem because this linear curve will be shifted left or right and also slightly change its slope depending on the temperature of the heater cartridge. If the cartridge is very cold, more energy is needed to heat up the liquid, i.e. the slope of the curve gets lower. Also, more heat is dissipated to the surrounding, i.e. the offset increases. Therefore, the heater temperature is also monitored.

The heater temperature saturates to a constant value after about 0.3 s. The evaporation has then reached a quasi-static regime where the heat flow into the liquid equals the evaporative heat loss. This temperature is monitored by averaging the temperature value for the period from 2 s to the end of the evaporation after 3 s. The resulting graph of average aerosol mass versus saturation temperature is shown in Fig 8.

A linear relation between saturation temperature and aerosol mass is clearly visible for temperatures higher than 210°C. This temperature measurement is independent on the ambient temperature as described earlier. The relation of saturation temperature to aerosol mass is also independent of the ambient temperature, as it only depends on the heat transfer between the MEMS heater and the evaporating liquid. The saturation temperature unfortunately varies for evaporations with the same heating power as indicated by the error bars. We believe that this variation is caused by the random formation of gas bubbles at the interface that alter the heat transfer.

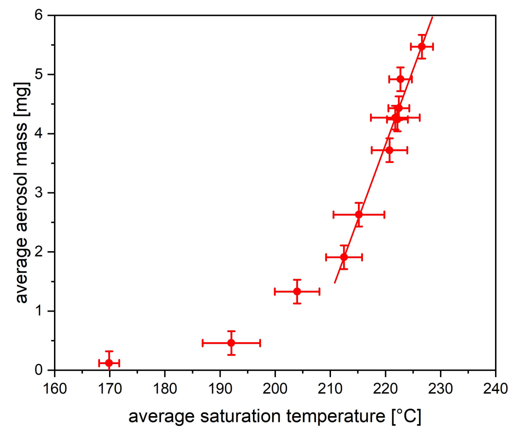

Figure 8: Average aerosol mass versus average saturation temperature for ten evaporation events with a duration of 3 s each.

This interpretation is supported by the slow variation of the heater temperature that is typically observed when driving the heater with the power regulation algorithm (Fig. 9). The curves for a constant power of 3.2 W differ by maximum of about 20 K and also the averaged saturation temperature varies between 203 °C and 216°C.

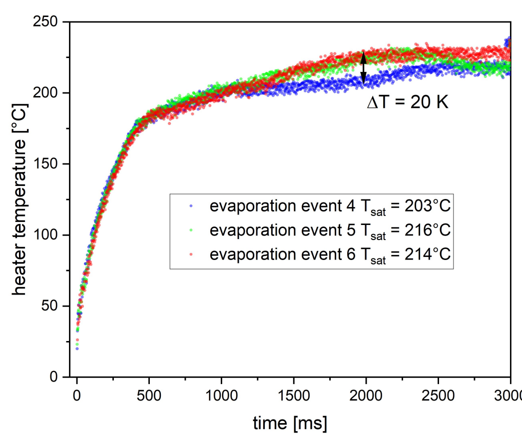

Figure 9: Typical heater temperature versus time characteristics of three successive evaporation events with power regulation

Fig. 10 shows a dosing event with four pre-set temperature values as an example of a temperature regulated dosing event. The temperature plateaus are much flatter compared to the characteristics of the power regulated characteristics from Fig 9. In turn, the instantaneous power varies to compensate for the varying heat transfer characteristic due to the bubbles at the heater interface.

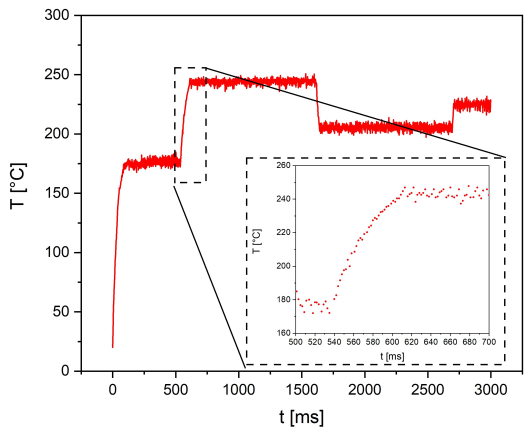

Figure 10: Heater temperature versus time characteristics of an evaporation event with four pre-set temperature values

The figure also demonstrates the fast heat-up and cool down phases of the MEMS heater. The fast heat-up is due to the power margin of the system. While the highest average power for a proper function is in the range of about 5 W, the maximum power for a hot heater (R = 1.2 Ω) with a battery voltage of 3.7 V is 11.4 W, which means that there is an extra power 6.4 W available for a fast heat up even in the boiling regime. The fast cooling down in the boiling regime is explained by the high power-loss due to evaporation. As no power is fed into the system while cooling down a power of several watts is dissipated by the evaporation.

CONCLUSION & OUTLOOK

We have shown two regulation schemes for the driving of a MEMS heater for evaporative drug delivery. First a power regulated scheme and second a temperature regulated scheme were demonstrated. With both driving schemes two parameters can be extracted to characterized the dosing event, the average power and the saturation temperature. Both parameters have their advantages and disadvantages for predicting the aerosol mass and therefore the delivered drug dose.

The average power is a precise measure of the delivered aerosol mass but only as long as the temperature of the cartridge and the surrounding is known. The saturation temperature on the other hand is a measure of the aerosol mass that is independent on the cartridge temperature and ambient temperature but suffers from a lower accuracy. We believe that a combination of both methods will lead to better prediction of the aerosol mass than each method alone.

Future work will concentrate on characterizing multiple cartridges with different ambient and cartridge temperatures and to find a reliable model that predict the administered drug dose on the basis of the average heating power, the saturation temperature and probably the ambient temperature.

ACKNOWLEDGEMENTS

We gratefully thank the Laboratory for Electrical Instrumentation and Embedded Systems for the opportunity to use their climate chamber.

REFERENCES

[1] Vazda, et.al, “Evaporation of fentanyl from ceramics for pulmonary drug delivery: a pilot study”, Conference on Materials Science and Engineering (2021)

[2] A. Vazda, Wei Xia, Håkan Engqvist, “The use of heat to deliver fentanyl via pulmonary drug delivery", International Journal of Pharmaceutics: X, Volume 3 (2021)

[3] K. Dinh et al., “In vitro aerosol characterization of Staccato® Loxapine”, Int. J. Pharm., 403 (2011)

[4] Pourchez, et al., "Assessment of new-generation high-power electronic nicotine delivery system as thermal aerosol generation device for inhaled bronchodilators", Int. J. Pharmaceutics, vol. 518, no. 1 (2017)

[5] F. Goldschmidtboeing et al., "Heater for Controlled Evaporation of Liquids for Personalized Drug Delivery to the Lungs," Journal of Microelectromechanical Systems, vol. 29, no. 5 (2020)

[6] https://www.pvlighthouse.com.au/resistivity, accessed January 13th, 2022

CONTACT

*Frank Goldschmidtboeing, tel: +49-761-203-7496; fgoldsch@imtek.de